© 2020. Published by The Company of Biologists Ltd | Journal of Experimental Biology (2020) 223, jeb210054. doi:10.1242/jeb.210054

METHODS & TECHNIQUES

In vitro virtual reality: an anatomically explicit musculoskeletal simulation powered by *in vitro* muscle using closed-loop tissue–software interaction

Christopher T. Richards* and Enrico A. Eberhard

ABSTRACT

Muscle force–length dynamics are governed by intrinsic contractile properties, motor stimulation and mechanical load. Although intrinsic properties are well characterised, physiologists lack *in vitro* instrumentation to account for combined effects of limb inertia, musculoskeletal architecture and contractile dynamics. We introduce *in vitro* virtual reality (*in vitro*-VR) which enables *in vitro* muscle tissue to drive a musculoskeletal jumping simulation. In hardware, muscle force from a frog plantaris was transmitted to a software model where joint torques, inertia and ground reaction forces were computed to advance the simulation at 1 kHz. To close the loop, simulated muscle strain was returned to update *in vitro* length. We manipulated (1) stimulation timing and (2) the virtual muscle's anatomical origin. This influenced interactions among muscular, inertial, gravitational and contact forces dictating limb kinematics and jump performance. We propose that *in vitro*-VR can be used to illustrate how neuromuscular control and musculoskeletal anatomy influence muscle dynamics and biomechanical performance.

KEY WORDS: Muscle mechanics, Force–length dynamics, Muscle physiology, Neuromuscular mechanics, Biomechanics, Frogs, Jumping, MuJoCo

INTRODUCTION

Skeletal muscle is astonishingly versatile. Despite its conserved contractile machinery across taxa (Lindstedt et al., 1998), a single muscle may shift from motor to brake, depending upon the relative timing of force and length patterns (Full et al., 1998; Ahn and Full, 2002; Ahn et al., 2006). Between these mechanical extremes, animals fine-tune muscle force–length dynamics to modulate mechanical power for running (e.g. Daley and Biewener, 2003; Gabaldón et al., 2004), swimming (e.g. Rome et al., 1993; Altringham and Johnston, 1990; Marsh et al., 1992; Richards and Biewener, 2007) or flying (e.g. Askew and Marsh, 2001; Ellerby and Askew, 2007; Morris and Askew, 2010). Our understanding of *in vivo* muscle versatility stems from *in vitro* experimentation where isolated tissue is stimulated at various fixed lengths (Ramsey and Street, 1940; Gordon et al., 1966), fixed loads (Hill, 1938) or fixed shortening–lengthening cycles (i.e. work loops; Pringle and Tregear, 1969; Josephson, 1985).

The above approaches are limited because mechanical loading is predetermined. Although changes in muscle stimulation can alter muscle work output, the fixed loading conditions do not permit variation in the acceleration trajectory of the load because length (or force) input is controlled at each time point. Hence, *in vitro* experiments can 'replay' mechanical events to mimic *in vivo* observations, but cannot explore how hypothetical changes in the neuro-musculoskeletal system might influence movements of the load. For example, rocket frogs achieve extreme jumps via both specialisations in contractile properties and increased tibia length (James and Wilson, 2008). Yet, although controlled-length experiments reveal how muscle properties confer power (Lutz and Rome, 1994), they cannot determine how bone morphology influences performance; changes in strain from concomitant shifts in leg posture, kinematics and muscle loading would be unknown and difficult to predict *a priori*.

Towards overcoming the predictive limitations of *in vitro* experimentation, pioneering studies used closed-loop force-feedback electronics to mimic the effects of varying inertial loads *in vitro* (Lin and Rymer, 1998, 2000) as well as to manipulate neuronal feedback *in vivo* (Sponberg et al., 2011). More recently, virtual reality environments have been developed into 'neuromorphic models' to interact with cadaver tissue (Niu et al., 2017) as well as simplified mechanical models to test effects of inertia, skeletal gearing and elasticity on *in vitro* muscle (Robertson and Sawicki, 2015; Sawicki et al., 2015). Building on those important 'virtual loading' techniques, as well as recent advances in muscle–hardware feedback (Richards, 2011; Richards and Clemente, 2012; Eberhard and Richards, 2018), we introduce *in vitro* virtual reality (*in vitro*-VR) as a hybrid of *in vitro* physiology (e.g. Lutz and Rome, 1994) and musculoskeletal simulation (Delp et al., 2007). *In vitro*-VR uses closed-loop feedback between simulation software and physiology hardware to cause an *in vitro* muscle to 'feel' immersed in a virtual reality environment. A crucial difference between *in vitro*-VR and previous methods is the incorporation of multibody dynamics and realistic ground contact forces. Thus, *in vitro*-VR has the potential to capture anatomical complexity (as does OpenSim) whilst additionally avoiding the pitfalls and oversimplifications of traditional muscle models (see Millard et al., 2019). For demonstration, we tested the effects of muscle stimulation versus altering limb anatomy by modifying the muscle's anatomical origin. We then describe the methodology and limitations as well as present data demonstrating *in vitro*-VR's utility for recording force–length dynamics in direct response to manipulating the virtual skeleton (e.g. muscle moment arms, limb inertia) towards a better understanding of how evolutionary transformations in limb architecture influence the mechanical demands of muscle.

MATERIALS AND METHODS

Instrumentation overview: a closed-loop hybrid simulator

In vitro-VR is a hybrid of two components, one part software and the other hardware. (A) A 2D musculoskeletal model of a jumping

The Royal Veterinary College, Hawkshead Lane, Hatfield AL9 7TA, UK.

*Author for correspondence (ctrichards@rvc.ac.uk)

C.T.R., 0000-0002-1908-3577

Received 5 July 2019; Accepted 20 March 2020

Journal of Experimental Biology (2020) 223, jeb210054. doi:10.1242/jeb.210054

frog is implemented in a software physics engine (MuJoCo; Todorov et al., 2012), which solves the forward dynamics equations to compute joint kinematics in response to joint torque inputs (Fig. 1A). (B) An *in vitro* muscle–tendon unit (MTU) is mounted to a custom ergometer (Richards and Clemente, 2012) instrumented with a 305C-LR muscle lever system (Aurora Scientific Ltd, Aurora, ON, Canada) which measures force at a controlled MTU length (Fig. 1B). In real time, components A and B form a closed-loop system; force recorded from B is transmitted to A, and converted to a joint torque via a moment arm r (see below), which causes joint acceleration. At each time step, acceleration is integrated to update instantaneous joint angles and MTU length. To close the loop, MTU length is transmitted back to B to update the instantaneous length of the real muscle tissue. Hence, the system uses a single experimental input (electrical stimulation to the muscle) and two primary measurements: muscle force (measured in B) and length change (computed in A).

In vitro-VR involves a chain of intercommunicating digital devices, each with latencies that ultimately limit the update rate of the closed loop. Two main latencies occur: simulation latency, which is the time required to perform forward dynamics calculations, and communication latency, which is the time required to read/write/convert digital information (see below). MuJoCo has been designed to run faster than real time (i.e. simulation latency is less than simulation time step) for robot control, which requires control signals to be computed/optimised predictively (Erez et al., 2013). Owing to the impressive performance of MuJoCo, simulation latency is tiny compared with communication latency, and hence the musculoskeletal simulation remains idle for the majority of the overall loop cycle. As explained below, communication lag is the rate-limiting step; therefore, the timing of digital communication was used to clock and synchronise all processes in the loop.

Our system architecture and software control minimises latencies among the system components, allowing the hardware–software loop to be updated at 1 kHz (see below). For our model, this update rate is sufficiently fast for muscle to smoothly 'feel' the resistance of the simulated limb via the amount of length change fed back through the system. For example, if the simulation encountered high resistance (e.g. a limb pulling a massive object), the resulting length change would be nearly zero at each time step. In contrast, for a low resistance (e.g. a limb moving through air), the muscle length change would be large. Importantly, we discuss (below) cases where 1 kHz is not sufficiently fast and suggest how to increase update rate.

Musculoskeletal simulation of a jumping frog

Despite the apparent simplicity of the overall system (Fig. 1A,B), muscle force–length dynamics emerge from a detailed computation performed in MuJoCo at each time step:

$$\mathbf{A} = \mathbf{M}^{-1}(\mathbf{T} + \mathbf{J}^{\mathrm{T}}\mathbf{F} - \mathbf{G}), \quad (1)$$

where $\mathbf{A}$ is the vector of n joint accelerations (n=number of joint degrees of freedom; n=4 in the current implementation), $\mathbf{M}$ is the mass–inertia matrix, $\mathbf{T}$ is the vector of joint torques, $\mathbf{F}$ is the contact force vector (e.g. ground reaction force) and $\mathbf{G}$ is gravity and Coriolis forces. A 'constraint Jacobian matrix', $\mathbf{J}$, maps contact forces to joint torques such that $\mathbf{J}^{\mathrm{T}}\mathbf{F}$ represents the joint torques required to resist a contact force vector acting on the limb (Todorov et al., 2012; see Richards, 2019, for a gentle introduction to multibody dynamics equations). We refer to 'internal' forces as $\mathbf{T}$ and $\mathbf{G}$ versus 'external' forces $\mathbf{J}^{\mathrm{T}}\mathbf{F}$, each in terms of joint torque (i.e. 'joint space').

In the current implementation, the jumper has a single leg with four planar hinge joints: tarso-metatarsal (TMT), ankle, knee and hip (Fig. 1A). Simplifications were made to allow the jumper to operate with a single extensor muscle (see below). The body segment masses and moments of inertia were determined from micro-computed tomography (μCT) image analysis of an 11.4 g *Kassina maculata* (walking/jumping frog) specimen as done previously (Porro et al., 2017; Richards et al., 2018). To extend the ankle and TMT joints, the plantaris muscle was modelled as a rigid cable originating at the knee and inserting on the proximal tarsals (Fig. 1A). Importantly, this 'cable' is not meant to represent rigid tissue properties, but rather serves as a placeholder which specifies the line of action along which muscle force is applied in simulation. Solid mass-less spheres on the joint centres allow the muscle path to curve smoothly around the joints without penetrating leg segments. At each simulation time step, MuJoCo's kinematics

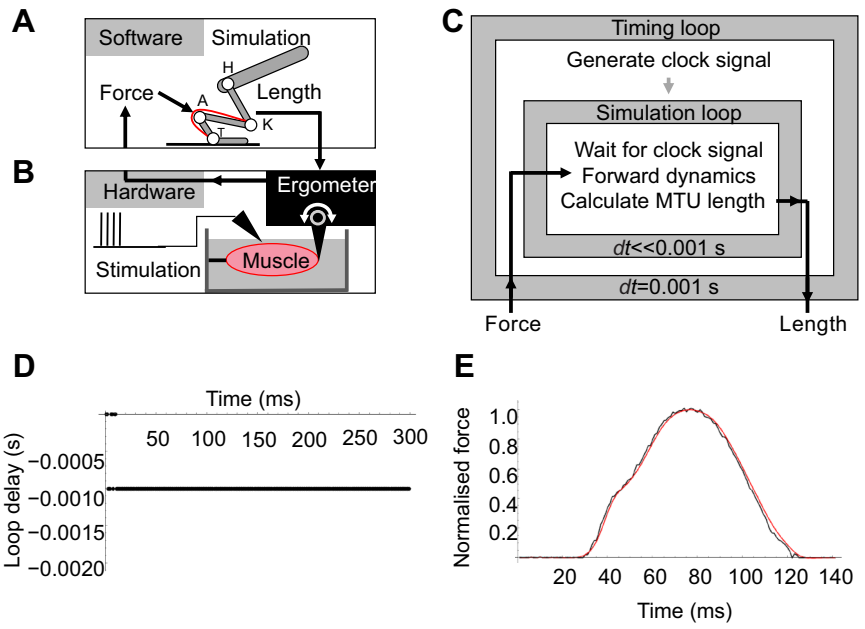

Fig. 1. Schematic diagrams and validation. The software simulation (A) in closed-loop feedback with the *in vitro* muscle ergometer (B), which electrically stimulates, measures force and imposes length changes on the muscle. A, ankle; K, knee; H, hip. The schematic diagram shows an outer timing loop controlling an inner simulation loop communicating in real time with the ergometer (C). MTU, muscle–tendon unit. Real-time function was confirmed by measuring the loop delay (D) and performing a 'communication loopback test' trial where force was recorded (black trace), then transmitted around the loop back to its origin and recorded again (red trace) to verify correct timing and fidelity of transmission (E).

Journal of Experimental Biology (2020) 223, jeb210054. doi:10.1242/jeb.210054

solver computes moment arms at the TMT and ankle. Consequently, the user does not assign moment arms directly; instead, they are computed based on the model's geometry and instantaneous posture. Note, however, that in the current model, the muscle path is constrained to wrap around the surface of a sphere, thus keeping moment arms nearly constant throughout the jumps. Future implementations could explore how time-varying moment arms might influence jumping (Roberts and Marsh, 2003). The simulated plantaris path represents a numerical placeholder for the *in vitro* muscle tissue. Although the plantaris contains fibres originating proximal to the knee (Dunlap, 1960), for simplicity, we defined the origin point precisely at the knee centre of rotation (i.e. the muscle produces no torque at the knee; we define this as the nominal condition). When the simulation runs, instantaneous *in vitro* muscle force enters the simulation as a scalar value which is applied along the spatial path of the modelled muscle to produce both ankle and TMT torque.

For the purposes of introducing our technique, thigh musculature was omitted and represented instead by lumped torque actuators at the hip and knee. During simulation, τ_{hip} and τ_{knee} are computed using simple proportional gain servos (see MuJoCo documentation; www.mujoco.org), producing torques to replicate hip and knee extension patterns from an exemplar jump recorded previously (Richards et al., 2017). Hence, hip and knee kinematics were programmed to remain consistent across simulation conditions, but ankle/TMT kinematics vary depending on emergent *in vitro* muscle dynamics. The torque vector, **T**, from Eqn 1 was thus determined as follows:

$$\mathbf{T} = [\tau_{TMT}, \tau_{ankle}, \tau_{knee}, \tau_{hip}], \quad (2)$$

$$\tau_{hip} = \text{gain}_{hip} e_{hip}, \quad (3)$$

$$\tau_{knee} = \text{gain}_{knee} e_{knee}, \quad (4)$$

$$\tau_{ankle} = f_{muscle} r_{ankle}, \quad (5)$$

$$\tau_{TMT} = f_{muscle} r_{TMT}, \quad (6)$$

where e is the difference between simulation joint angle and the experimentally recorded angle, and gains are arbitrary servo gains set in the MuJoCo model parameters.

In vitro measurement of muscle force

Although our current model is implemented based on *K. maculata*, we used muscle isolated from similar-sized *Xenopus laevis* to develop and demonstrate the *in vitro*-VR technique. Future use of this technique to evaluate jumping performance in *K. maculata* will employ muscle isolated from *K. maculata* specimens. We stress that the current study used a muscle from this non-specialised jumper only to demonstrate the technique. For the present purposes, we wish to illustrate how real muscle (as opposed to a Hill-type muscle model) can be coupled to a simulation to yield interesting biological insights. However, we also note that anuran muscle properties have been shown to vary across species (Astley, 2016); thus, inter-species effects are likely to be important and should be explored in the future.

An adult male *X. laevis* was weighed then killed using 2 g l^{-1} solution of tricaine methanesulfonate (MS-222; Sigma-Aldrich, Dorset, UK) followed by removal of the heart, according to a UK Home Office Licence (70/8242). The plantaris longus muscle was removed, mounted to the ergometer and bathed with standard oxygenated saline solution maintained at 22°C and augmented with $CaCl_2$ (1.3 mmol l^{-1} Ca^{2+}) and glucose (10 mmol l^{-1}). Tissue preparation is detailed in prior work (Richards and Clemente, 2012, 2013). Briefly, using repeated twitch contractions, stimulation voltage was increased until maximum isometric force was achieved. Subsequently, optimal length (24.08 mm) was found by adjusting passive tension until the muscle produced the highest force (approximating the plateau of the force–length relationship; Richards and Clemente, 2013). Prior to experimental trials, the mass of the current frog specimen (30.3 g) was used to scale the mass/inertia parameters of the MuJoCo frog model (11.4 g) using isometric scaling such that the mass of the model matched that of the real frog specimen whilst maintaining proportions. For frog jumps, the muscle was stimulated at maximal voltage at a spike frequency known to produce maximum force for *X. laevis* (250 Hz; Richards, 2011). Foot contact time for *K. maculata* ranges between ~80 and 200 ms (Porro et al., 2017); thus, a stimulation duration of 80 ms was selected based on the lower bound of this observed range. Note, however, that no attempt was made in the current study to maximise muscle force, which would probably occur at longer stimulation durations. The muscle was allowed to rest for at least 5 min between contractions.

Control loop architecture, communication and timing

In principle, there are many ways to achieve closed-loop hardware–software feedback for *in vitro*-VR. For the current implementation, two loops were used: a simulation loop (inner loop) running an instance of MuJoCo and a timing loop (outer loop) generating 1 kHz clock signals (Fig. 1C). A schematic diagram showing hardware parts and wiring is shown in Fig. S1. The code for the current implementation can be found from an online repository (https://github.com/frogtronics/InvitroVR).

The simulation loop has the following sequence of events, where MuJoCo performs the following: (1) joint angles are updated (based on integrated accelerations from the previous time step); (2) moment arms and muscle lengths are computed; (3) *in vitro* force is substituted into Eqns 5 and 6, and hip/knee servo torques are computed; (4) internal forces are calculated; (5) external forces are solved (e.g. ground reaction force); (6) Eqn 1 is integrated to advance the simulation by one timestep (dt=1 ms) to give the current simulation time (t=t+dt); and (7) simulation state (positions, angles) is stored in a buffer for later saving.

When a clock signal is received from the timing loop, the simulation loop returns to step 1 to repeat the computation sequence. In the current application, steps 1–7 are completed rapidly (<<1 ms) before the simulation loop waits idle for a clock signal to return to step 1.

In addition to fast computation, *in vitro*-VR requires fast communication between analog (muscle ergometer) and digital hardware (PC). To avoid confusion, input/output will be discussed with respect to the musculoskeletal simulation (in the PC), which receives muscle force input and produces a muscle length output. Analog/digital (A/D:D/A) conversion, device communication, synchronisation and timing were achieved with a high performance Arduino (Arduino Due; 84 MHz 32-bit ARM core microcontroller; Arduino, Somerville, MA, USA). A National Instruments NI-6289 data acquisition system (DAQ; National Instruments, Austin, TX, USA) generates the stimulation pulses to the muscle whilst synchronously recording analog data output from the ergometer at the same rate as the loop (1 kHz). The DAQ runs 'outside' the control loop; it operates deterministically in parallel with the microcontroller, but is independent from any computation/communication latencies in the loop. Thus, the DAQ could be used as an independent measure of 'real world' time. For best performance, MuJoCo should run on a dedicated PC (or processor core) whilst the DAQ and Arduino software run on a separate PC. Additionally, a field-programmable

Journal of Experimental Biology (2020) 223, jeb210054. doi:10.1242/jeb.210054

gate array (FPGA; Compact Rio 9074; National Instruments) runs at 10 kHz to perform three tasks. (1) It applies a second-order low-pass Butterworth filter set at 60 Hz and 100 Hz for length and force signals, respectively. (2) The FPGA also performs voltage matching between devices to allow the signals from the Arduino to drive the muscle lever (see Fig. S1). (3) The FPGA checks the validity of the signals and enables/disables the ergometer accordingly (see code repository; https://github.com/frogtronics/InvitroVR).

Most importantly, transmissions among the devices must be synchronised such that the time elapsed in the simulation (t_{sim}) matches time elapsed in the real world (t_{real}). Precisely, for every millisecond elapsed in the real world, the simulation must advance exactly one time step, regardless of the computation time of the simulator. Given that loop rate is limited by communication latencies, synchronisation can be achieved by precise timing of data transmission from the microcontroller to the PC. Specifically, the simulation only advances after receiving a valid signal from the microcontroller which is precisely clocked by a built-in interrupt timer. All digital data were packaged as ASCII characters in binary form and tagged with an 'end-of-transmission' code, which validates the data then signals the simulation to proceed. Because MuJoCo is not run deterministically in the current implementation, simulation latency can vary depending on processes that are currently running in the operating system. Before conducting experimental trials, loop delay should be measured (Fig. 1D). Most importantly, a lookback test was performed; the simulation transmitted the force signal as output (instead of length) to verify that an analog signal can travel entirely around the loop without being altered by simulation/communication latencies or by conversion errors (Fig. 1E). Additionally, each trial recorded values of t_{sim} (from MuJoCo) and t_{real} (ground truth time from the operating system) as separate data streams to verify *post hoc* that $t_{sim}=t_{real}$. Together, these validations confirm correct timing (i.e. hardware/software running at the same rate), correct synchronisation (i.e. same start time) and fidelity (i.e. no numerical errors in ASCII decoding or transmission beyond precision/resolution limits).

Overall sequence of events in the hardware–software loop

(1) First, the user initialises the system: the DAQ system is enabled, an instance of MuJoCo is started, the microcontroller establishes an RS-232 link to the PC (and vice versa) and the microcontroller initialises a 1 kHz clock. Once the system is enabled, the microcontroller begins listening for analog force data from the ergometer as well as for valid digital length data from the PC. The simulation is paused at $t_{sim}=t_{real}=0$. (2) The user presses a hardware trigger to initiate the timing loop. (3) The microcontroller converts an analog force signal (from the ergometer force output) to digital then writes the data to the serial RS-232 port of the PC. (4) The PC continuously reads data from the incoming RS-232 port until valid force data are received from the microcontroller then decoded from binary ASCII characters to a floating point force value. This event triggers a single iteration of the simulation loop. (5) The simulation loop advances (see sequence above). (6) The PC converts the instantaneous MTU length (computed from the simulation) to digital and writes the data to the outgoing RS-232 port. (7) The microcontroller reads the MTU length data and decodes it to a floating point value then scales the value using a calibration factor and offset appropriate for the ergometer hardware. (8) The microcontroller writes the MTU length value to the analog output, which is transmitted to the length input of the ergometer hardware. (9) If t_{sim} is less than the specified end of simulation (e.g. 0.5 s), the loop returns to step 3. (10) After completion of the simulation, a reset sequence is initiated which automatically returns muscle length to its initial value and resets all software values to their nominal values. (11) Buffered simulation data are saved to file. The DAQ saves all data recorded from analog channels.

Experimental procedure

To demonstrate the method, we performed five arbitrary experimental conditions: (1) a nominal condition where the muscle was stimulated 20 ms following the onset of hip and knee extension, (2) a control condition (control 1) where the plantaris muscle was absent from the simulation, (3) a passive condition (control 2) where the muscle was included in the simulation, but not stimulated (and thus could produce passive force), (4) a nominal condition but with stimulation onset beginning 60 ms following proximal joint motion and (5) a modified anatomical condition where the virtual origin of the plantaris (in simulation) was switched to a proximal location on the femur to cause knee flexor action from plantaris contraction. The nominal condition is based on a well-established observation that frogs extend their proximal joints earlier in jumps (e.g. Calow and Alexander, 1973). Control 1 and 2 are theoretical conditions to verify that the simulation is dependent upon feedback from the real muscle. The conditions for delayed stimulation and modified anatomy (conditions 4 and 5, above) are arbitrary hypothetical conditions to demonstrate how the technique is sensitive to changes in neural stimulation as well as changes in anatomy. Across all conditions, the stimulation burst and the hip/knee kinematics were held constant.

Limitations of the *in vitro*-VR method

A fundamental limitation of *in vitro* muscle measurements is that traditional stimulation of the whole muscle or whole nerve cannot replicate *in vivo* activation where motor units are independently activated according to the mechanical demands of a task (Hodson-Tole and Wakeling, 2009). In the future, one could incorporate sophisticated stimulation electrode designs (e.g. Branner et al., 2001) towards a more physiological stimulation pattern. All other limitations are with regard to anatomical complexity. Our system design only allows a single muscle to be tested in a given closed-loop system. However, additional loops could be easily linked in parallel (each with its own dedicated processor core). This would allow multiple *in vitro* muscles (each mounted to its own ergometer) to dynamically interact as they each attach (virtually) to a simulated limb. An additional limitation is the lack of tendon dynamics. In future implementations, the user can attach in-series tendons to *in vitro* muscles by adding spring elements emulated in software. Finally, the present implementation assumes that muscle fascicle strain is identical to whole-muscle strain. In the future, one could use sonomicrometry to measure and control fascicle length using an inner control loop (Robertson et al., 2017).

Performance limits of the current implementation and how to overcome them

This section discusses the principal system limitations of the current implementation and suggests modifications for improved performance for future implementations of *in vitro*-VR. The four principal limitations to *in vitro*-VR are: (1) maximum speed of the analog ergometer hardware, (2) minimum/maximum numerical range and resolution (i.e. digits of precision for floating point force/length values), (3) loop rate (1/maximum latency) and (4) simulation rate. Firstly, the ergometer motor (Aurora 305C-LR), depending on damping, has a maximum speed of ~400 mm s^{-1}, which far exceeds the maximum speed of muscle contraction in most applications, and thus is a negligible limitation.

Journal of Experimental Biology (2020) 223, jeb210054. doi:10.1242/jeb.210054

For example, a 2 cm muscle will reach 200 mm s^{-1} at a contractile speed of 10 lengths s^{-1}. In rare cases where faster lever movements are required, the system can be tuned with higher gain settings (at the expense of damping). Secondly, both numerical precision and minimum/maximum range are limited by the resolution of A/D:D/A converters in the loop. Currently, we use the built-in converters on the microcontroller, which operate between 0 and ∼2.2 V (after accounting for a DC offset). The converters are 12-bit allowing the range of 2.2 V to be divided into 4096 levels, giving a numerical precision of 2.2/4096 V, which is sufficiently fine for the current application. Given that our ergometer was calibrated at 1 V=1 N, our muscle force limit was 2.2 N, which was sufficient for the size of the muscle used currently. However, for applications with larger muscles producing force in excess of 2.2 N, either the force would require attenuation or an alternative microcontroller would be used. Thirdly, as stated above, communication latency dominates our implementation. At each time step, the microcontroller/PC must use serial communication to transmit/receive 12-bit values. The speed bottleneck of our current implementation is the PC operating system (64-bit Windows 7) which permits a maximum RS-232 baud rate of 115,200 bits s^{-1}. Combining all delays (four read–write operations, MuJoCo computations and other operations), the maximum overall loop rate of the current system is between 1 and 2 kHz; thus, we used 1 kHz for safe operation. If the system were too slow and/or of low resolution, the muscle would 'feel' coarse and grainy motion versus smooth. Additionally, force would oscillate, which can be seen in slower feedback systems (see fig. 2A from Richards, 2011, which suffered from a 2 ms delay). Neither 'graininess' nor oscillations were observed in the current implementation, indicating that 1 kHz is sufficiently fast for loads produced at the time scales of a frog jump. Finally, simulation rate must be considered. Although the current implementation is relatively simple (four joints and one contact), more complex simulations could increase simulation latency which could invalidate the dynamics because muscle force would not correspond to simulation acceleration. In principle, additional degrees of freedom increase the complexity of the multibody dynamics. In practice, MuJoCo can handle extreme anatomical complexity (at least 1000-fold greater complexity than the current model) whilst maintaining a simulation latency less than 1 ms (see http://www.mujoco.org/performance.html). We note, however, that contacts and collisions occurring at rapid time scales may significantly slow computation time. For example, we speculate that a large quadruped in a gallop could be extremely challenging to simulate with sufficiently low latency. Future modelling studies would be required to evaluate how model and contact complexity influences simulation latency.

In future implementations, the system performance can be improved. Although 1 kHz allows smooth operation for the current model, it would probably be too slow to model tendon recoil dynamics or for faster dynamics of extremely small frogs. The rate could be increased easily with faster serial communication afforded by increasing the baud rate or by using an alternative communication protocol (e.g. ethernet; Eberhard and Richards, 2018). A faster processor and use of multiple processor cores would increase the speed by orders of magnitude (see http://www.mujoco.org/performance.html). If resolution were limiting (not currently the case), higher quality converters (e.g. 16-bit or higher) would massively increase the numerical precision along with better electronics to improve signal to noise ratio. For future implementations, a deterministic real-time operating system (RTOS) would provide a crucial improvement of performance. Otherwise, the user cannot precisely control the priority of computational processes; an unrelated process (e.g. a software update or virus scan, etc.) may slow computations or communication. Because a true RTOS was not used for the present study, we were required to verify that the control loop was timed correctly to maintain a constant loop rate (Fig. 1D,E). If other processes were running, the loop rate would potentially be time varying rather than constant, rendering the simulation results difficult to interpret.

RESULTS AND DISCUSSION

In vitro-VR measures *in vitro* force in response to simulated gravity, inertia and contacts

We measured force and length changes of a muscle responding to simulated inertial and ground reaction forces of a jumping frog within a real-time simulator. Data for all trials are given in Table S1.

Simulated jump trajectory was highly dependent on muscle stimulation conditions as well as muscle anatomy (Fig. 2). To our knowledge, this is the first study to connect an *in vitro* muscle to an anatomically explicit musculoskeletal simulation using closed-loop feedback. For simplicity and to introduce the technique, we used a single muscle with a 2D simulation. No attempts were made to adjust experimental conditions to produce maximal jumping performance. Future implementations can easily incorporate 3D dynamics and additional muscles 'in the loop' (see Materials and Methods) as well as controllers to optimise joint kinematics.

At the onset of all jumps, the simulation initially sank towards the ground as a result of gravity causing a brief period of joint flexion and muscle lengthening (Fig. 3). Soon thereafter, hip, knee, ankle and TMT joint accelerations acted to extend the leg to propel the body upwards and forwards as the plantaris shortened. Two controls were used to verify that real-time muscle simulation feedback influenced jump performance. In control 1 (muscle absent) the leg extended, but jumped only weakly (Movie 1; Fig. 2C). In this case, intersegmental forces among the body segments caused the ankle to extend in the absence of muscle force. This transfer of motion among segments is a crucial, but often under-appreciated phenomenon of multi-body dynamic systems (Kuo, 2001) which would be missed if the mass/inertia of the leg were neglected using simpler modelling and *in vitro* approaches. Motion transfer occurs as a result of intersegmental forces at the joints; these forces implicitly act as constraint forces attaching each segment to the next (i.e. allowing rotation, but preventing translation). In control 2 (muscle present, but unstimulated), initial joint flexion caused muscle stretching, which produced passive force and ankle extensor torque. This passive force acted like an elastic cable to transmit intersegmental forces from proximal joint extension to the ground. Consequently, the foot produced sufficient ground reaction force to lift the frog farther from the simulated floor compared with control 1 (Movie 2). For subsequent trials with electrically stimulated muscle, the simulation jumped at least twice the height observed for control jumps (Figs 2D and 3; Movie 3). These trials confirm that the closed-loop real-time feedback allows the muscle to influence the simulation and vice versa.

To further demonstrate the utility of *in vitro*-VR, we altered musculoskeletal anatomy by altering the origin of the plantaris muscle (Fig. 2B). In the nominal case, the plantaris origin was positioned at the knee to eliminate any action about this joint (see Materials and Methods). We explored the effects of editing musculoskeletal architecture by shifting the origin proximally to a point above the knee. This manipulation allowed the plantaris to act at the knee as a flexor, causing dramatic alterations to plantaris force–length dynamics. Rather than a brief period of lengthening followed by a large degree of shortening, the muscle remained nearly isometric then shortened shallowly (Fig. 3B). As the knee

Journal of Experimental Biology (2020) 223, jeb210054. doi:10.1242/jeb.210054

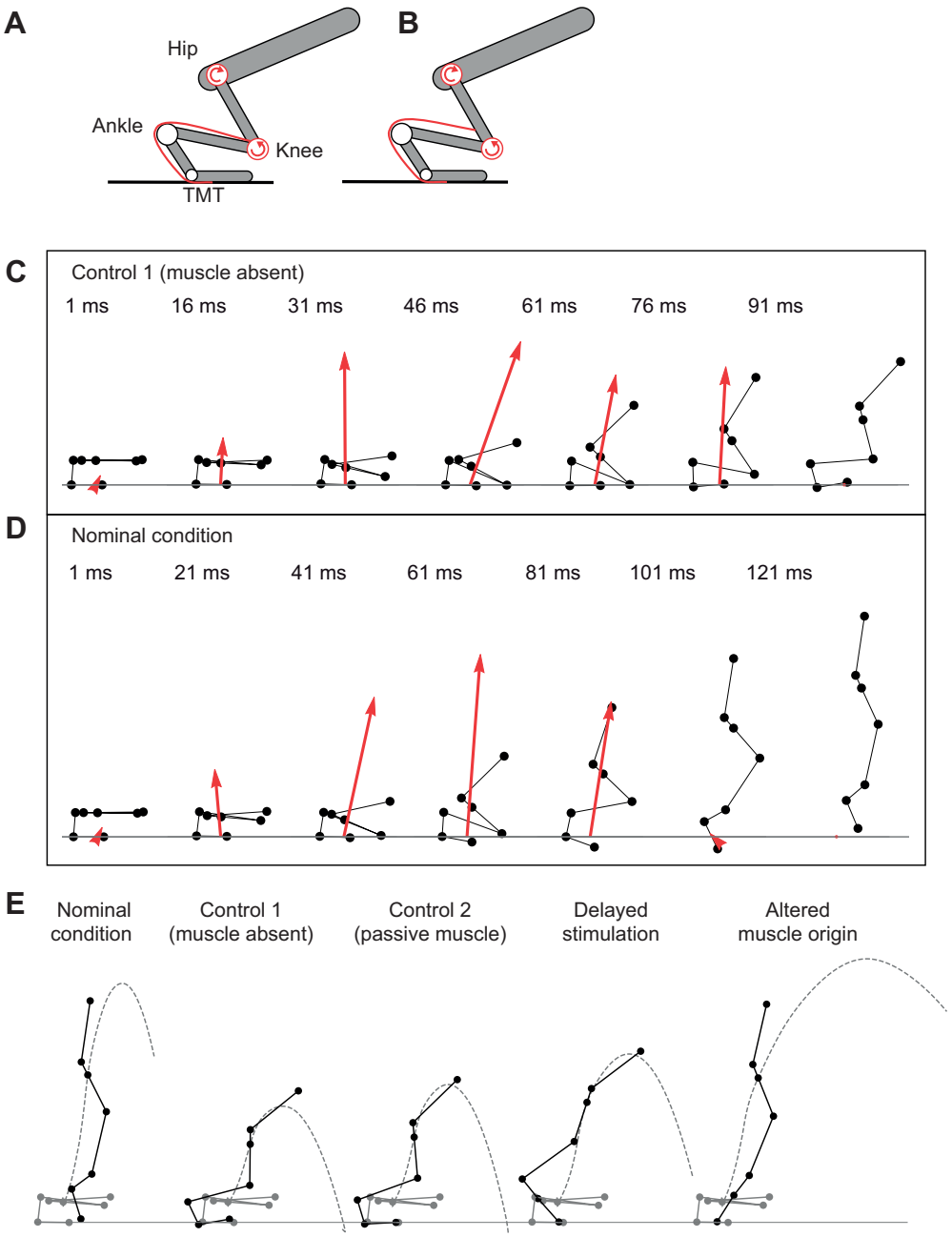

Fig. 2. Experimental conditions and simulated jump performance. Schematic diagram of nominal anatomy (A) versus a muscle origin shifted proximally to induce a biarticular action at the knee (B). The hip and knee joints are modelled as torque actuators (red curved arrows), whereas torque at the ankle and tarso-metatarsal (TMT) emerge from force produced along the path of the plantaris muscle (red line). Jump kinematics are shown for control 1 (plantaris muscle absent; C) versus the nominal condition (D). The red arrow is the ground reaction force vector. Jump trajectories (E) are shown (dashed grey line) for five experimental conditions (see Materials and Methods). Stick figures of the jumper are shown at 20 ms (grey) and at the time of takeoff (black).

extended it acted as an antagonist to the plantaris such that the shortening that would have occurred was instead cancelled by the upward rotation of the femur to 'pull' on the muscle origin. Consequently, the plantaris briefly acted as a strut to transmit force to the ankle. In this special case, knee extension is 'transferred' to the ankle via a bi-articular link, allowing the ankle to extend with minimal plantaris shortening. Exploring the full dynamic consequences of this shift in force–length dynamics is beyond the scope of the current work as it requires further investigation using a range of incremental anatomical changes as well as a sweep of stimulation conditions. Regardless, for the purposes of demonstrating the technique, *in vitro*-VR offers intriguing direct evidence that changes in musculoskeletal architecture can greatly influence muscle function, independently of neural stimulation.

In vitro-VR is complementary to traditional *in vitro* experimentation

In vitro experimentation, particularly the work-loop method (Pringle and Tregear, 1969; Josephson, 1985), enables exploration of parameters to map muscle 'performance space' relating force, work and power to strain and stimulation patterns (Josephson, 1985; Altringham and Johnston, 1990; Luiker and Stevens, 1993). One can then ask further questions: why do muscles operate within a particular region in their performance space?; why do muscles perform maximally under some conditions (e.g. Rome et al., 1993), but sub-maximally under others (Tu and Daniel, 2004)? These questions require modelling the physical forces resisting muscle contraction (Marsh, 1999). In some cases, simple modelling can demonstrate how 'environmental feedback' (Aerts and Nauwelaerts, 2009) can reduce

Journal of Experimental Biology (2020) 223, jeb210054. doi:10.1242/jeb.210054

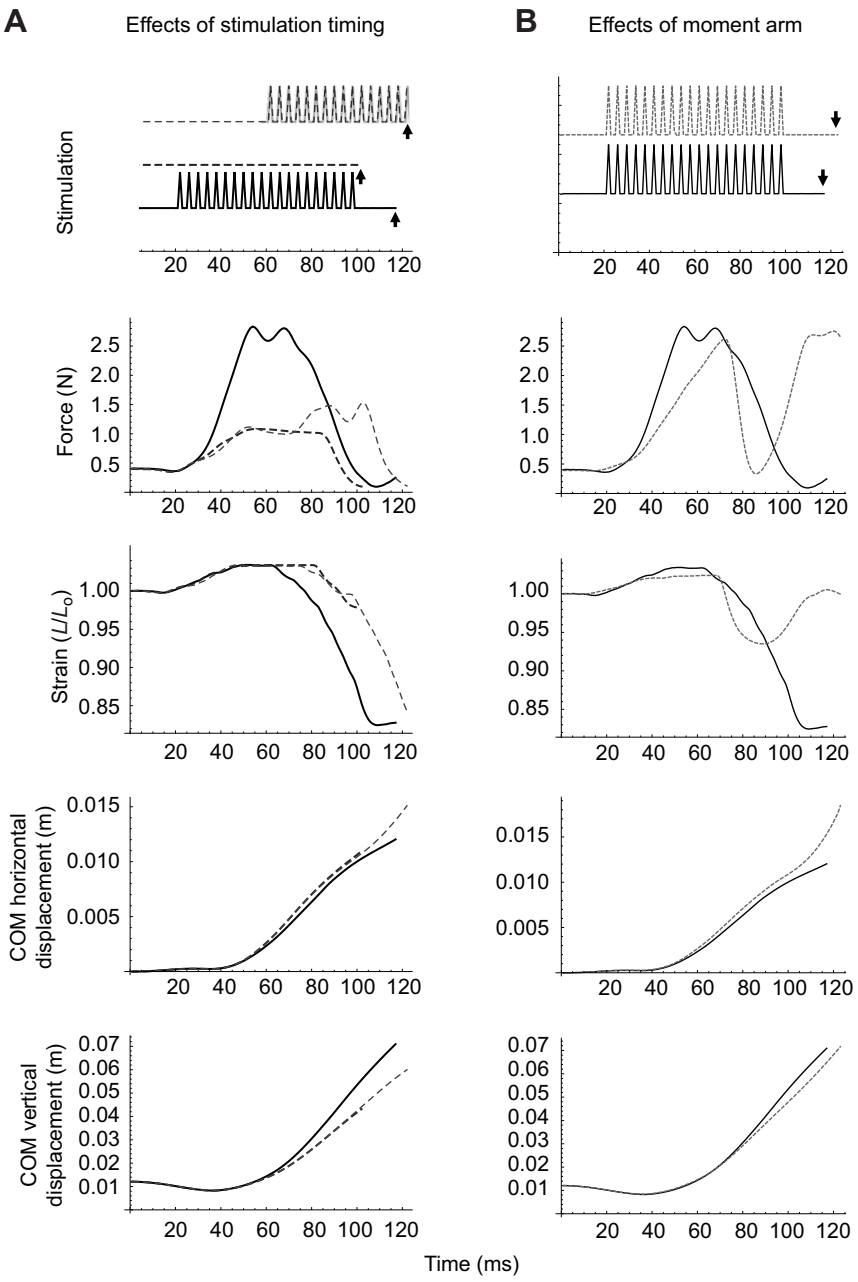

Fig. 3. *In vitro* force–length dynamics and simulated jumping performance. Timing of muscle stimulation was varied (A). Nominal simulation (solid black lines) is compared with control 1 (dashed black lines) versus delayed onset of stimulation (dashed grey lines). Moment arm was varied (B) to show differences in dynamics due to applying a flexor moment at the knee. The nominal simulation with no knee action (solid black line; as in A) is compared with a simulation where the plantaris is biarticular at the knee (dashed grey line). Note that different simulation conditions affect the timing of takeoff; data are only shown prior to takeoff (arrows in top panel). COM, centre of mass. Note also that muscle length data (L) are normalised by resting muscle length (L_o).

the 'volume' of muscle performance space (Richards, 2011; Richards and Clemente, 2013; Clemente and Richards, 2013). In other cases, for example in swimming fish, sophisticated modelling is required to reveal how optimal muscle function is dependent upon the mechanical properties of the body, which governs fluid–structure interactions (Tytell et al., 2010). Unfortunately, however, modelling struggles to capture the full richness of muscle function observed during active lengthening (as reviewed by Herzog, 2014; Nishikawa, 2016) or extremely rapid events such as 'short-range' length perturbations (Millard et al., 2019). Consequently, traditional Hill-type models will fail to explain rapid force–velocity transients occurring on millisecond time scales crucial in behaviours such as ballistic tongue projection in frogs (Lappin et al., 2006) or the response to unexpected perturbations in running birds (Daley et al., 2006, 2009).

In light of the above shortcomings of muscle modelling approaches, there are large gaps between our understanding of *in vitro* contractile dynamics and *in vivo* function at the organismal level. We propose *in vitro*-VR can help close this gap by measuring muscle force–length dynamics in response to an arbitrarily realistic model of limb anatomy, inertia and substrate contact. In essence, *in vitro*-VR directly measures aspects that remain poorly characterised and are challenging to model (i.e. tissue dynamics) whilst simulating the remaining parameters that can be modelled and validated more easily (multibody and contact dynamics). We make a crucial point that *in vitro*-VR does not replace traditional *in vitro* experimentation; the methods are complementary. *In vitro* experiments such as work loops reveal the full performance space of muscle whilst *in vitro*-VR explains how anatomy and environment limit *in vivo* operation within this space.

Applications of *in vitro*-VR

In vitro-VR can provide unique insights into several current problems. Firstly, several researchers have refined the Hill-type muscle model (Gordon et al., 1966; Hill, 1938); however, muscle models are difficult to validate outside of standard protocols where

parameters are held fixed. *In vitro*-VR can produce contractile dynamics closer to *in vivo* conditions because the dynamic loads relate directly to limb function observed in natural behaviour (i.e. activation, velocity and force each vary simultaneously). Thus, *in vitro*-VR could help validate recent muscle models accounting for traditionally neglected features such as the role of titin to explain history-dependent effects (Nishikawa et al., 2011) as well as 'short-range' impedance effects (Millard et al., 2019), tissue mass (Günther et al., 2012; Ross and Wakeling, 2016) and 3D structure (Blemker and Delp, 2005; Ross et al., 2018). Secondly, *in vitro* techniques have established how force is enhanced through stimulation timing (e.g. Burke et al., 1970; Sandercock and Heckman, 1997), active stretching (Edman et al., 1978) and starting length (Azizi and Roberts, 2010). *In vitro*-VR can be used to determine whether these well-established effects are likely to occur *in vivo* and whether they enhance performance during a complex behaviour. Thirdly, *in vitro*-VR can be an important tool to understand how muscle–tendon systems 'amplify' muscle power for propulsion (Peplowski and Marsh, 1997) or 'attenuate' power for braking (Ahn et al., 2006; Richards and Sawicki, 2012; Konow and Roberts, 2015), depending on loading and posture (Galantis and Woledge, 2003; Roberts and Marsh, 2003) as well as substrate properties (Reynaga et al., 2019). Our method could further elucidate how dynamic inertial effects of multi-body systems (Richards, 2019) influence these loading and substrate effects. Finally, *in vitro*-VR could be used to directly measure the functional consequences of anatomical changes occurring over evolutionary time (e.g. Emerson, 1979; Reilly and Jorgensen, 2011) or due to ecological factors (e.g. Louppe et al., 2017).

Conclusion

We present a technique, *in vitro*-VR, which aims to advance *in vitro* muscle physiology and musculoskeletal simulation (e.g. Delp et al., 2007) by creating a novel link between the two approaches. *In vitro* experimentation enables physiologists to control neuromuscular stimulation and strain patterns to help determine how the nervous system modulates mechanical work and power. In addition to stimulation, *in vitro*-VR allows manipulation of limb anatomy and locomotor substrate. When traditional methods and *in vitro*-VR experimentation are applied in tandem, one can probe how anatomy and locomotor environment influence the mechanical demands on a muscle *in vivo*. One can address new questions, such as: how does anatomy or substrate influence the mapping between motor stimulation and mechanical output? Additionally, the present method has wider applications; for example, to test tissue samples affected by disease or injury to better isolate and understand their effects on locomotion. Hence, we propose *in vitro*-VR is a broadly applicable method within and beyond the comparative/evolutionary context.

Acknowledgements

We greatly thank Tim West for advice on muscle preparation, and assistance with laboratory setup and buffer solutions. We also thank Rue Jones for donating to us a small number of *Xenopus* frogs for this study. Cameron Hill assisted with equipment testing and Chris Basu and two anonymous reviewers provided helpful comments on the manuscript.

Competing interests

The authors declare no competing or financial interests.

Author contributions

Conceptualization: C.T.R., E.A.E.; Methodology: C.T.R., E.A.E.; Software: C.T.R., E.A.E.; Validation: C.T.R.; Formal analysis: C.T.R.; Investigation: C.T.R.; Resources: C.T.R.; Data curation: C.T.R.; Writing - original draft: C.T.R.; Writing - review & editing: C.T.R.; Visualization: C.T.R.; Supervision: C.T.R.; Project administration: C.T.R.; Funding acquisition: C.T.R.

Funding

This work was funded by a European Research Council Starting Grant (PIPA 338271).

Data availability

Code is available from our github repository: https://doi.org/10.5281/zenodo.3759379.

Supplementary information

Supplementary information available online at http://jeb.biologists.org/lookup/doi/10.1242/jeb.210054.supplemental

References

Aerts, P. and Nauwelaerts, S. (2009). Environmentally induced mechanical feedback in locomotion: Frog performance as a model. *J. Theor. Biol.* **261**, 372-378. doi:10.1016/j.jtbi.2009.07.042

Ahn, A. N. and Full, R. J. (2002). A motor and a brake: two leg extensor muscles acting at the same joint manage energy differently in a running insect. *J. Exp. Biol.* **205**, 379-389.

Ahn, A. N., Meijer, K. and Full, R. J. (2006). In situ muscle power differs without varying in vitro mechanical properties in two insect leg muscles innervated by the same motor neuron. *J. Exp. Biol.* **209**, 3370-3382. doi:10.1242/jeb.02392

Altringham, J. D. and Johnston, I. A. (1990). Scaling effects on muscle function: power output of isolated fish muscle fibers performing oscillatory work. *J. Exp. Biol.* **151**, 453-467.

Askew, G. N. and Marsh, R. L. (2001). The mechanical power output of the pectoralis muscle of blue-breasted quail (Coturnix chinensis): the in vivo length cycle and its implications for muscle performance. *J. Exp. Biol.* **204**, 3587-3600.

Astley, H. C. (2016). The diversity and evolution of locomotor muscle properties in anurans. *J. Exp. Biol.* **219**, 3163-3173. doi:10.1242/jeb.142315

Azizi, E. and Roberts, T. J. (2010). Muscle performance during frog jumping: influence of elasticity on muscle operating lengths. *Proc. Biol. Sci.* **277**, 1523-1530. doi:10.1098/rspb.2009.2051

Blemker, S. S. and Delp, S. L. (2005). Three-dimensional representation of complex muscle architectures and geometries. *Ann. Biomed. Eng.* **33**, 661-673. doi:10.1007/s10439-005-1433-7

Branner, A., Stein, R. B. and Normann, R. A. (2001). Selective stimulation of cat sciatic nerve using an array of varying-length microelectrodes. *J. Neurophysiol.* **85**, 1585-1594. doi:10.1152/jn.2001.85.4.1585

Burke, R. E., Rudomin, P. and Zajac, F. E. (1970). Catch property in single mammalian motor units. *Science* **168**, 122-124. doi:10.1126/science.168.3927.122

Calow, L. and Alexander, R. McN. (1973). A mechanical analysis of a hind limb of a frog. *J. Zool. Lond.* **171**, 292-321. doi:10.1111/j.1469-7998.1973.tb05341.x

Clemente, C. J. and Richards, C. (2013). Muscle function and hydrodynamics limit power and speed in swimming frogs. *Nature Comm.* **4**, 1-8. doi:10.1038/ncomms3737

Daley, M. A. and Biewener, A. A. (2003). Muscle force-length dynamics during level versus incline locomotion: a comparison of in vivo performance of two guinea fowl ankle extensors. *J. Exp. Biol.* **206**, 2941-2958. doi:10.1242/jeb.00503

Daley, M. A., Usherwood, J. R., Felix, G. and Biewener, A. A. (2006). Running over rough terrain: guinea fowl maintain dynamic stability despite a large unexpected change in substrate height. *J. Exp. Biol.* **209**, 171-187. doi:10.1242/jeb.01986

Daley, M. A., Voloshina, A. and Biewener, A. A. (2009). The role of intrinsic muscle mechanics in the neuromuscular control of stable running in the guinea fowl. *J. Physiol.* **587**, 2693-2707. doi:10.1113/jphysiol.2009.171017

Delp, S. L., Anderson, F. C., Arnold, A. S., Loan, P., Habib, A., John, C. T., Guendelman, E. and Thelen, D. G. (2007). OpenSim: open-source software to create and analyze dynamic simulations of movement. *IEEE Trans. Biomed. Eng.* **54**, 1940-1950. doi:10.1109/TBME.2007.901024

Dunlap, D. G. (1960). The comparative myology of the pelvic appendage in the Salientia. *J. Morphol.* **106**, 1-76. doi:10.1002/jmor.1051060102

Eberhard, E. A. and Richards, C. T. (2018, July). Simulation of muscle-powered jumping with hardware-in-the-loop ground interaction. In 2018 IEEE/ASME International Conference on Advanced Intelligent Mechatronics (AIM) (pp. 201-206). IEEE.

Edman, K. A. P., Elzinga, G. and Noble, M. I. M. (1978). Enhancement of mechanical performance by stretch during tetanic contractions of vertebrate skeletal muscle fibres. *J. Physiol.* **281**, 139-155. doi:10.1113/jphysiol.1978.sp012413

Ellerby, D. J. and Askew, G. N. (2007). Modulation of flight muscle power output in budgerigars Melopsittacus undulatus and zebra finches Taeniopygia guttata: in vitro muscle performance. *J. Exp. Biol.* **210**, 3780-3788. doi:10.1242/jeb.006288

Emerson, S. B. (1979). The ilio-sacral articulation in frogs: form and function. *Biol. J. Linn. Soc.* **11**, 153-168. doi:10.1111/j.1095-8312.1979.tb00032.x

Erez, T., Lowrey, K., Tassa, Y., Kumar, V., Kolev, S. and Todorov, E. (2013). An integrated system for real-time model predictive control of humanoid robots. In 2013 13th IEEE-RAS International Conference on Humanoid Robots (Humanoids) (pp. 292-299). IEEE.

Full, R. J., Stokes, D. R., Ahn, A. N. and Josephson, R. K. (1998). Energy absorption during running by leg muscles in a cockroach. *J. Exp. Biol.* **201**, 997-1012.
Gabaldón, A. M., Nelson, F. E. and Roberts, T. J. (2004). Mechanical function of two ankle extensors in wild turkeys: shifts from energy production to energy absorption during incline versus decline running. *J. Exp. Biol.* **207**, 2277-2288. doi:10.1242/jeb.01006
Galantis, A. and Woledge, R. C. (2003). The theoretical limits to the power output of a muscle–tendon complex with inertial and gravitational loads. *Proc. R. Soc. London. Ser. B Biol. Sci.* **270**, 1493-1498. doi:10.1098/rspb.2003.2403
Gordon, A. M., Huxtey, A. F. and Jitliant, F. J. (1966). The variation in isometric tension with sarcomere length in vertebrate muscle fibres. *J. Physiol.* **184**, 170-192. doi:10.1113/jphysiol.1966.sp007909
Günther, M., Röhrle, O., Haeufle, D. F. and Schmitt, S. (2012). Spreading out muscle mass within a Hill-type model: a computer simulation study. *Comput. Math. Methods Med.* **2012**, 848630. doi:10.1155/2012/848630
Herzog, W. (2014). Mechanisms of enhanced force production in lengthening (eccentric) muscle contractions. *J. Appl. Physiol.* **116**, 1407-1417. doi:10.1152/japplphysiol.00069.2013
Hill, A. V. (1938). The heat of shortening and the dynamic constants of muscle. *Proc. R. Soc. London. Ser. B Biol. Sci.* **126**, 136-195. doi:10.1098/rspb.1938.0050
Hodson-Tole, E. F. and Wakeling, J. M. (2009). Motor unit recruitment for dynamic tasks: current understanding and future directions. *J. Comp. Physiol. B* **179**, 57-66. doi:10.1007/s00360-008-0289-1
James, R. S. and Wilson, R. S. (2008). Explosive jumping: extreme morphological and physiological specializations of Australian rocket frogs (Litoria nasuta). *Physiol. Biochem. Zool.* **81**, 176-185. doi:10.1086/525290
Josephson, R. (1985). The mechanical power output from striated muscle during cyclic contraction. *J. Exp. Biol.* **114**, 493-512.
Konow, N. and Roberts, T. J. (2015). The series elastic shock absorber: tendon elasticity modulates energy dissipation by muscle during burst deceleration. *Proc. R. Soc. B* **282**, 20142800. doi:10.1098/rspb.2014.2800
Kuo, A. D. (2001). The action of two-joint muscles: the legacy of WP Lombard. *Classics Mov. Sci.* 289-316.
Lappin, A. K., Monroy, J. A., Pilarski, J. Q., Zepnewski, E. D., Pierotti, D. J. and Nishikawa, K. C. (2006). Storage and recovery of elastic potential energy powers ballistic prey capture in toads. *J. Exp. Biol.* **209**, 2535-2553. doi:10.1242/jeb.02276
Lin, D. C. and Rymer, W. Z. (1998). Damping in reflexively active and areflexive lengthening muscle evaluated with inertial loads. *J. Neurophysiol.* **80**, 3369-3372. doi:10.1152/jn.1998.80.6.3369
Lin, D. C. and Rymer, W. Z. (2000). Damping actions of the neuromuscular system with inertial loads: soleus muscle of the decerebrate cat. *J. Neurophysiol.* **83**, 652-658. doi:10.1152/jn.2000.83.2.652
Lindstedt, S. L., McGlothlin, T., Percy, E. and Pifer, J. (1998). Task-specific design of skeletal muscle: balancing muscle structural composition. *Comp. Biochem. Physiol. B Biochem. Mol. Biol.* **120**, 35-40. doi:10.1016/S0305-0491(98)00021-2
Louppe, V., Courant, J. and Herrel, A. (2017). Differences in mobility at the range edge of an expanding invasive population of Xenopus laevis in the west of France. *J. Exp. Biol.* **220**, 278-283. doi:10.1242/jeb.146589
Luiker, E. A. and Stevens, E. D. (1993). Effect of stimulus train duration and cycle frequency on the capacity to do work in the pectoral fin muscle of the pumpkinseed sunfish, Lepomis gibbosus. *Can. J. Zool.* **71**, 2185-2189. doi:10.1139/z93-307
Lutz, G. J. and Rome, L. C. (1994). Built for jumping: the design of the frog muscular system. *Science (80-.)* **263**, 370-372. doi:10.1126/science.8278808
Marsh, R. L. (1999). How muscles deal with real-world loads: the influence of length trajectory on muscle performance. *J. Exp. Biol.* **202**, 3377-3385.
Marsh, R. L., Olson, J. M. and Guzik, S. K. (1992). Mechanical performance of scallop adductor muscle during swimming. *Nature* **357**, 411-413. doi:10.1038/357411a0
Millard, M., Franklin, D., Herzog, W. (2019). A continuous and differentiable mechanical model of muscle force and impedance. In *Wearable Robotics: Challenges and Trends* (ed. M. Carrozza, S. Micera and J. Pons). WeRob 2018. Biosystems & Biorobotics, vol 22, pp. 262-266. Springer. doi:10.1007/978-3-030-01887-0_50
Morris, C. R. Askew, G. N. (2010). The mechanical power output of the pectoralis muscle of cockatiel (Nymphicus hollandicus): the in vivo muscle length trajectory and activity patterns and their implications for power modulation. *J. Exp. Biol.* **213**, 2770-2780. doi:10.1242/jeb.035691
Nishikawa, K. (2016). Eccentric contraction: unraveling mechanisms of force enhancement and energy conservation. *J. Exp. Biol.* **219**, 189-196. doi:10.1242/jeb.124057
Nishikawa, K. C., Monroy, J. A., Uyeno, T. E., Yeo, S. H., Pai, D. K. and Lindstedt, S. L. (2011). Is titin a 'winding filament'? A new twist on muscle contraction. *Proc. R. Soc. B* **279**, 981-990. doi:10.1098/rspb.2011.1304
Niu, C. M., Jalaleddini, K., Sohn, W. J., Rocamora, J., Sanger, T. D. and Valero-Cuevas, F. J. (2017). Neuromorphic meets neuromechanics, part I: the methodology and implementation. *J. Neural Eng.* **14**, 025001. doi:10.1088/1741-2552/aa593c
Peplowski, M. M. and Marsh, R. L. (1997). Work and power output in the hindlimb muscles of Cuban tree frogs Osteopilus septentrionalis during jumping. *J. Exp. Biol.* **200**, 2861-2870.
Porro, L. B., Collings, A. J., Eberhard, E. A., Chadwick, K. P. and Richards, C. T. (2017). Inverse dynamic modelling of jumping in the red-legged running frog Kassina maculata. *J. Exp. Biol.* **220**, 1882-1893. doi:10.1242/jeb.155416
Pringle, J. W. S. and Tregear, R. T. (1969). Mechanical properties of insect fibrillar muscle at large amplitudes of oscillation. *Proc. R. Soc. Lond. B Biol. Sci.* **174**, 33-50. doi:10.1098/rspb.1969.0079
Ramsey, R. W. and Street, S. F. (1940). The isometric length-tension diagram of isolated skeletal muscle fibers of the frog. *J. Cell. Comp. Physiol.* **15**, 11-34. doi:10.1002/jcp.1030150103
Reilly, S. M. and Jorgensen, M. E. (2011). The evolution of jumping in frogs: morphological evidence for the basal anuran locomotor condition and the radiation of locomotor systems in crown group anurans. *J. Morphol.* **272**, 149-168. doi:10.1002/jmor.10902
Reynaga, C. M., Eaton, C. E., Strong, G. A. and Azizi, E. (2019). Compliant substrates disrupt elastic energy storage in jumping tree frogs. *Integr. Comp. Biol.* **59**, 1535-1545.doi:10.1093/icb/icz069
Richards, C. T. (2011). Building a robotic link between muscle dynamics and hydrodynamics. *J. Exp. Biol.* **214**, 2381-2389. doi:10.1242/jeb.056671
Richards, C. T. (2019). Energy flow in multibody limb models: a case study in frogs. *Integr. Comp. Biol.* **59**, 1559-1572. doi:10.1093/icb/icz142
Richards, C. T. and Biewener, A. A. (2007). Modulation of in vivo muscle power output during swimming in the African clawed frog (Xenopus laevis). *J. Exp. Biol.* **210**, 3147-3159. doi:10.1242/jeb.005207
Richards, C. T. and Clemente, C. J. (2012). A bio-robotic platform for integrating internal and external mechanics during muscle-powered swimming. *Bioinspir. Biomim.* **7**, 16010. doi:10.1088/1748-3182/7/1/016010
Richards, C. T. and Clemente, C. J. (2013). Built for rowing: frog muscle is tuned to limb morphology to power swimming. *J. R Soc. Interface* **10**, 20130236. doi:10.1098/rsif.2013.0236
Richards, C. T. and Sawicki, G. S. (2012). Elastic recoil can either amplify or attenuate muscle–tendon power, depending on inertial vs. fluid dynamic loading. *J. Theor. Biol.* **313**, 68-78. doi:10.1016/j.jtbi.2012.07.033
Richards, C. T., Porro, L. B. and Collings, A. J. (2017). Kinematic control of extreme jump angles in the red-legged running frog, Kassina maculata. *J. Exp. Biol.* **220**. doi:10.1242/jeb.144279
Richards, C. T., Eberhard, E. A. and Collings, A. J. (2018). The dynamic role of the ilio-sacral joint in jumping frogs. *Biol. Lett.* **14**, 20180367. doi:10.1098/rsbl.2018.0367
Roberts, T. J. and Marsh, R. L. (2003). Probing the limits to muscle-powered accelerations: lessons from jumping bullfrogs. *J. Exp. Biol.* **206**, 2567-2580. doi:10.1242/jeb.00452
Robertson, B. D. and Sawicki, G. S. (2015). Unconstrained muscle-tendon workloops indicate resonance tuning as a mechanism for elastic limb behavior during terrestrial locomotion. *Proc. Natl Acad. Sci. USA* **112**, E5891-E5898. doi:10.1073/pnas.1500702112
Robertson, B., Vadakkeveedu, S. and Sawicki, G. S. (2017). A benchtop biorobotic platform for in vitro observation of muscle-tendon dynamics with parallel mechanical assistance from an elastic exoskeleton. *J. Biomech.* 57, 8-17. doi:10.1016/j.jbiomech.2017.03.009
Rome, L. C., Swank, D. and Corda, D. (1993). How fish power swimming. *Science (80-.)* **261**, 340-342. doi:10.1126/science.8332898
Ross, S. A. and Wakeling, J. M. (2016). Muscle shortening velocity depends on tissue inertia and level of activation during submaximal contractions. *Biol. Lett.* **12**, 20151041. doi:10.1098/rsbl.2015.1041
Ross, S. A., Nigam, N. and Wakeling, J. M. (2018). A modelling approach for exploring muscle dynamics during cyclic contractions. *PLOS Comput. Biol.* **14**, e1006123. doi:10.1371/journal.pcbi.1006123
Sandercock, T. G. and Heckman, C. J. (1997). Doublet potentiation during eccentric and concentric contractions of cat soleus muscle. *J. Appl. Physiol.* **82**, 1219-1228. doi:10.1152/jappl.1997.82.4.1219
Sawicki, G. S., Sheppard, P. and Roberts, T. J. (2015). Power amplification in an isolated muscle–tendon unit is load dependent. *J. Exp. Biol.* **218**, 3700-3709. doi:10.1242/jeb.126235
Sponberg, S., Libby, T., Mullens, C. H. and Full, R. J. (2011). Shifts in a single muscle's control potential of body dynamics are determined by mechanical feedback. *Philos. Trans. R. Soc. Lond. B. Biol. Sci.* **366**, 1606-1620. doi:10.1098/rstb.2010.0368
Todorov, E., Erez, T. and Tassa, Y. (2012, October). Mujoco: A physics engine for model-based control. In 2012 IEEE/RSJ International Conference on Intelligent Robots and Systems (pp. 5026-5033). IEEE.
Tu, M. S. and Daniel, T. L. (2004). Submaximal power output from the dorsolongitudinal flight muscles of the hawkmoth Manduca sexta. *J. Exp. Biol.* **207**, 4651-4662. doi:10.1242/jeb.01321
Tytell, E. D., Hsu, C.-Y., Williams, T. L., Cohen, A. H. and Fauci, L. J. (2010). Interactions between internal forces, body stiffness, and fluid environment in a neuromechanical model of lamprey swimming. *Proc. Natl. Acad. Sci. USA* **107**, 19832-19837. doi:10.1073/pnas.1011564107